

Vortex chains induced by anisotropic spin-orbit coupling and magnetic field in spin-2 Bose-Einstein condensates

Hao Zhu(朱浩), Shou-Gen Yin(印寿根), and Wu-Ming Liu(刘伍明)
Citation: Chin. Phys. B, 2022, 31 (**6**): 060305. DOI: 10.1088/1674-1056/ac4020
Journal homepage: http://cpb.iphy.ac.cn; http://iopscience.iop.org/cpb

What follows is a list of articles you may be interested in

Supersymmetric structures of Dirac oscillators in commutative and noncommutative spaces

Jing-Ying Wei(魏静莹), Qing Wang(王青), and Jian Jing(荆坚)
Chin. Phys. B, 2021, 30 (**11**): 110307. DOI: 10.1088/1674-1056/ac05ab

Preparation of a two-state mixture of ultracold fermionic atoms with balanced population subject to the unstable magnetic field

Donghao Li(李东豪), Lianghui Huang(黄良辉), Guoqi Bian(边国旗), Jie Miao(苗杰), Liangchao Chen(陈良超), Zengming Meng(孟增明), Wei Han(韩伟), and Pengjun Wang(王鹏军)
Chin. Phys. B, 2021, 30 (**9**): 090303. DOI: 10.1088/1674-1056/abee6e

Influences of spin-orbit interaction on quantum speed limit and entanglement of spin qubits in coupled quantum dots

M Bagheri Harouni
Chin. Phys. B, 2021, 30 (**9**): 090301. DOI: 10.1088/1674-1056/abeef4
Noah F. Q. Yuan
Chin. Phys. B, 2021, 30 (**7**): 070311. DOI: 10.1088/1674-1056/ac00a3

Nonlocal advantage of quantum coherence and entanglement of two spins under intrinsic decoherence

Bao-Min Li(李保民), Ming-Liang Hu(胡明亮), and Heng Fan(范桁)
Chin. Phys. B, 2021, 30 (**7**): 070307. DOI: 10.1088/1674-1056/abff2a

Thermodynamic properties of massless Dirac-Weyl fermions under the generalized uncertainty principle

Guang-Hua Xiong(熊光华), Chao-Yun Long(龙超云), and He Su(苏贺)
Chin. Phys. B, 2021, 30 (**7**): 070302. DOI: 10.1088/1674-1056/abe1aa

---

Vortex chains induced by anisotropic spin–orbit coupling and magnetic field in spin-2 Bose–Einstein condensates

Hao Zhu(朱浩)[1], Shou-Gen Yin(印寿根)[1,†], and Wu-Ming Liu(刘伍明)[2,3,4,‡]

[1] *Key Laboratory of Display Materials and Photoelectric Devices (Ministry of Education), Tianjin Key Laboratory for Photoelectric Materials and Devices, School of Materials Science and Engineering, Tianjin University of Technology, Tianjin* 300384, *China*

[2] *Beijing National Laboratory for Condensed Matter Physics, Institute of Physics, Chinese Academy of Sciences, Beijing* 100190, *China*

[3] *School of Physical Sciences, University of Chinese Academy of Sciences, Beijing* 100190, *China*

[4] *Songshan Lake Materials Laboratory, Dongguan* 523808, *China*

(Received 16 November 2021; revised manuscript received 3 December 2021; accepted manuscript online 5 December 2021)

We investigate the anisotropic spin–orbit coupled spin-2 Bose–Einstein condensates with Ioffe–Pritchard magnetic field. With nonzero magnetic field, anisotropic spin–orbit coupling will introduce several vortices and further generate a vortex chain. Inside the vortex chain, the vortices connect to each other, forming a line along the axis. The physical nature of the vortex chain can be explained by the particle current and the momentum distribution. The vortex number inside the vortex chain can be influenced via varying the magnetic field. Through adjusting the anisotropy of the spin–orbit coupling, the direction of the vortex chain is changed, and the vortex lattice can be triggered. Moreover, accompanied by the variation of the atomic interactions, the density and the momentum distribution of the vortex chain are affected. The realization and the detection of the vortex chain are compatible with current experimental techniques.

Keywords: vortex chain, anisotropic spin–orbit coupling, magnetic field, Bose–Einstein condensates

PACS: 03.75.Lm, 03.75.Hh, 03.75.Nt, 05.30.Jp **DOI:** 10.1088/1674-1056/ac4020

1. Introduction

Vortices, vortex chains and vortex lattices have constituted the most relevant topological nontrivial excitations in the condensed matter physics.[1–3] These topological excitations contain phase singularities in the phase field, which can be characterized by winding numbers.[4–6] Usually, vortices are relevant to the external rotation of fluid, i.e., water[7] or superfluid.[8] Vortices have already been predicted or realized in the superfluid phase of ^{4}He.[9–11] Remarkably, vortices are opined to be the key point to some foundations of the systems, such as magnetic materials,[12–14] quantum memories,[15–17] and quantum optics.[18–20] Among the plethora of several physical systems, the highly controllable ultracold bosonic gases open a new gate of engineering nontrivial excitations.[21] Therefore, substantial investigations on the vortex generation,[22] the dynamic evolution[23] and the stability[24] have been executed in the field of Bose–Einstein condensations (BECs). To investigate the quantum vortices and superfluidity in the spinor BECs, external rotation often plays an important role.[25] In physics, rotation can be characterized by nonzero canonical angular momentum $\langle L_z^c \rangle = \int \boldsymbol{\Psi}^\dagger (\boldsymbol{r} \times \hat{\boldsymbol{p}}) \boldsymbol{\Psi} \, \mathrm{d}\boldsymbol{r}$.[26–29] And vortices are generated in response to the canonical angular momentum.[28,29] The common ways to rotate the condensates, including stirring the condensate[30] or rotating the anisotropic trap,[31] could introduce canonical angular momentum. However, with the help of gauge field and magnetic field, nonzero canonical angular momentum can also be generated.[28]

Recent investigations on artificial gauge field, i.e., spin–orbit coupling (SOC) techniques[32–34] in spinor BECs have attracted tremendous interest in systematically studying the novel vortex structures hosted by spinor BECs. For example, Xu *et al*. have found that Rashba-type SOC could trigger a one-dimensional (1D) vortex chain in spin-1/2 BECs.[35] The anisotropic SO-coupled BECs were firstly discussed by Stanescu *et al*.,[36] and the ground-state phase diagrams are found to have much richer structures than those obtained by using external rotation.[37] In spin-2 BECs, anisotropic SOC can be used to generate various patterns in the cyclic phase.[38] Furthermore, it is interesting to explore how SOC could generate novel vortex configurations other than the SOC itself.[39] Accompanied by the Ioffe–Pritchard (IP) magnetic field, Dresselhaus-type SOC could trigger vortex lattices in spin-1/2 BECs without external rotation.[28] Various nontrivial excitations, i.e., strip phase and vortex-ring phase, have been investigated with the combined effects of rotation, magnetic field or isotropic SOC in the low-spin systems.[40,41] However, the exotic vortex configurations in the ferromagnetic phase, anti-ferromagnetic phase or the cyclic phase of the spin-2 BECs system remain unclear.

In this paper, we apply anisotropic SOC to trigger 1D vortex chain in the spin-2 BECs. Magnetic field and anisotropic SOC are applied to replace the external rotation, introducing

†Corresponding author. E-mail: sgyin@tjut.edu.cn

‡Corresponding author. E-mail: wmliu@iphy.ac.cn

© 2022 Chinese Physical Society and IOP Publishing Ltd

angular momentum to the system. When magnetic field is absent, the 1D SOC (along the x-direction) can induce the plane wave phase ground state. However, the x-axis distributed vortex chain is generated by the combined effect of 1D SOC and magnetic field. Through calculating the particle current and the momentum distribution, we find that the 1D vortex chain is formed attributing to two contrary-propagated plane waves. Through changing the magnetic field, the vortex number inside of the vortex chain is varied. When keep the y-direction SOC zero, the vortex number inside of the vortex chain would increase with the x-direction SOC strength. However, when keep the x-direction SOC strength at a fixed value, vortex lattices and y-axis distributed vortex chains can be generated by increasing the y-direction SOC strength. Moreover, the influence of the spin-exchange interaction and the spin singlet-pairing interaction of the vortex chain and the vortex lattice is investigated.

This paper is organized as follows. We firstly introduce the model Hamiltonian in Section 2. The mean-field ground state solution of the x-axis distributed vortex chain is obtained by numerical minimizing the Hamiltonian function, and the particle current and momentum distribution of the vortex chain are discussed in Subsection 3.1. The influence of magnetic field on the vortex chain is discussed in Subsection 3.2. Moreover, we investigate the influence of anisotropic SOC effect on the vortex chain in Subsection 3.3. To connect with real experiments, we discuss the atomic interaction effect on the vortex chain and the lattice in Subsection 3.4. Eventually, Section 4 is devoted to concluding remarks.

2. Gross–Pitaevskii eqnarray

We consider a two-dimensional (2D) spin-2 BECs with the combined effect of anisotropic SOC and IP magnetic field. The mean-field Hamiltonian can be depicted as[42–44]

$$\begin{aligned}\mathcal{H} =& \int \mathrm{d}\boldsymbol{r}\boldsymbol{\Psi}^{\dagger}\bigg(-\frac{\hbar^2}{2m}\nabla^2+\mathcal{V}_{\mathrm{H}}+\mathcal{V}_{\mathrm{SO}}+\mu_{\mathrm{B}}g_{\mathrm{F}}\boldsymbol{B}\cdot\boldsymbol{F}\bigg)\boldsymbol{\Psi}\\&+\int \mathrm{d}\boldsymbol{r}\bigg(\frac{c_0}{2}\boldsymbol{\rho}^2+\frac{c_1}{2}\mid\boldsymbol{F}\mid^2+\frac{c_2}{2}\mid\boldsymbol{\Theta}\mid^2\bigg),\end{aligned}\tag{1}$$

where $\boldsymbol{\Psi}=[\Psi_2(\boldsymbol{r}),\Psi_1(\boldsymbol{r}),\Psi_0(\boldsymbol{r}),\Psi_{-1}(\boldsymbol{r}),\Psi_{-2}(\boldsymbol{r})]$ characterizes the macroscopic wave function of the condensate. m is the atomic mass and $n=\sum_l n_l=\sum_l|\Psi_l|^2$ is the total particle density, where $l=\pm2,\pm1,0$. The 2D wave functions are normalized as $\int n\ \mathrm{d}x\mathrm{d}y=N$. The harmonic potential is $\mathcal{V}_{\mathrm{H}}=\frac{1}{2}m\omega_{\perp}^2(x^2+y^2)$, μ_{B} is Bohr magneton, and $g_{\mathrm{F}}=-1/2$ is the Landé g_{F} factor. The strengths of the density–density interaction, the spin-exchange interaction and the spin singlet-pairing interaction are $c_0=2\hbar^2(4a_2+3a_4)/(7m)$, $c_1=2\hbar^2(a_4-a_2)/(7m)$ and $c_2=2\hbar^2(7a_0-10a_2+3a_4)/(7m)$, respectively, where a_0, a_2 and a_4 represent the s-wave scattering lengths in total spin $f_{\mathrm{tot}}=0$, 2 and 4 channels.[45] $\boldsymbol{F}=(F_x,F_y,F_z)=(\boldsymbol{\Psi}^{\dagger}\hat{F}_x\boldsymbol{\Psi},\boldsymbol{\Psi}^{\dagger}\hat{F}_y\boldsymbol{\Psi},\boldsymbol{\Psi}^{\dagger}\hat{F}_z\boldsymbol{\Psi})$ with spin-2 matrices $\hat{F}_{x,y,z}$, and $\boldsymbol{\Theta}=c_2(2\psi_2\psi_{-2}-\psi_1\psi_{-1}+\psi_0^2)/5$ is the amplitude of the spin singlet-pair. The anisotropic SOC term can be characterized as $\mathcal{V}_{\mathrm{SO}}=-\mathrm{i}\hbar(\kappa_xF_x\hat{\partial}_x+\kappa_yF_y\hat{\partial}_y)$, where κ_x and κ_y are SOC strength in the x and y directions.[46] The external IP magnetic field is depicted as $\boldsymbol{B}(\boldsymbol{r})=B(x\hat{x}-y\hat{y})$, where B is the radial field gradient in the x–y plane, and $\hat{x},\hat{y}$ are the unit vectors along the x,y directions, respectively.[47] For numerical calculation, it is convenient to make the following parameter transformations:

$$\begin{aligned}&x=\xi_0\tilde{x},\quad y=\xi_0\tilde{y},\quad t=\omega_{\perp}^{-1}\tilde{t},\\&\kappa_{x,y}=\sqrt{(\hbar\omega_{\perp})/m}\tilde{\kappa}_{x,y},\quad B=\hbar\omega_{\perp}/(\mu_{\mathrm{B}}g_{\mathrm{F}}\xi_0)\tilde{B},\\&\Psi_l=\sqrt{N}\xi_0^{-1}\tilde{\Psi}_l,\quad c_{0,1,2}=4\pi N\tilde{c}_{0,1,2},\end{aligned}\tag{2}$$

where the length of the trap unit is $\xi_0=\sqrt{\hbar/m\omega_{\perp}}$. In the mean-field approximation, the spin-2 BECs can be described by the following dimensionless Gross–Pitaevskii (GP) equations:[42–44]

$$\begin{aligned}\mathrm{i}\frac{\partial\tilde{\Psi}_{\pm2}}{\partial\tilde{t}}=&\bigg[-\frac{1}{2}\tilde{\nabla}^2+\tilde{V}_{\mathrm{ext}}+\tilde{c}_0\tilde{n}\bigg]\tilde{\Psi}_{\pm2}\\&+\frac{\tilde{c}_2}{\sqrt{5}}\tilde{\Theta}\tilde{\Psi}_{\mp2}^{\dagger}+\tilde{c}_1(\tilde{F}_{\mp}\tilde{\Psi}_{\pm1}\pm2\tilde{F}_z\tilde{\Psi}_{\pm2})\\&+(-\mathrm{i}\tilde{\kappa}_x\partial_x\mp\tilde{\kappa}_y\partial_y)\Psi_{\pm1}+\mathrm{i}\tilde{B}(\tilde{x}\pm\mathrm{i}\tilde{y})\tilde{\Psi}_{\pm1},\end{aligned}\tag{3}$$

$$\begin{aligned}\mathrm{i}\frac{\partial\tilde{\Psi}_{\pm1}}{\partial\tilde{t}}=&\bigg[-\frac{1}{2}\tilde{\nabla}^2+\tilde{V}_{\mathrm{ext}}+\tilde{c}_0\tilde{n}\bigg]\tilde{\Psi}_{\pm1}-\frac{\tilde{c}_2}{\sqrt{5}}\tilde{\Theta}\tilde{\Psi}_{\mp1}^{\dagger}\\&+\tilde{c}_1\bigg(\frac{\sqrt{6}}{2}\tilde{F}_{\mp}\tilde{\Psi}_0+\tilde{F}_{\pm}\tilde{\Psi}_{\pm2}\pm\tilde{F}_z\tilde{\Psi}_{\pm1}\bigg)\\&+\bigg(-\mathrm{i}\tilde{\kappa}_x\partial_x\pm\tilde{\kappa}_y\partial_y\bigg)\Psi_{\pm2}+\frac{\sqrt{6}}{2}(-\mathrm{i}\tilde{\kappa}_x\partial_x\mp\tilde{\kappa}_y\partial_y)\Psi_0\\&+\mathrm{i}\tilde{B}(\tilde{x}\mp\mathrm{i}\tilde{y})\tilde{\Psi}_{\pm2}+\frac{\sqrt{6}}{2}\mathrm{i}\tilde{B}(\tilde{x}\pm\mathrm{i}\tilde{y})\tilde{\Psi}_0,\end{aligned}\tag{4}$$

$$\begin{aligned}\mathrm{i}\frac{\partial\tilde{\Psi}_0}{\partial\tilde{t}}=&\bigg[-\frac{1}{2}\tilde{\nabla}^2+\tilde{V}_{\mathrm{ext}}+\tilde{c}_0\tilde{n}\bigg]\tilde{\Psi}_0+\frac{\tilde{c}_2}{\sqrt{5}}\tilde{\Theta}\tilde{\Psi}_0^{\dagger}\\&+\frac{\sqrt{6}}{2}\tilde{c}_1(\tilde{F}_-\tilde{\Psi}_{-1}+\tilde{F}_+\tilde{\Psi}_1)+\frac{\sqrt{6}}{2}(-\mathrm{i}\tilde{\kappa}_x\partial_x+\tilde{\kappa}_y\partial_y)\Psi_1\\&+\frac{\sqrt{6}}{2}(-\mathrm{i}\tilde{\kappa}_x\partial_x-\tilde{\kappa}_y\partial_y)\Psi_{-1}-\frac{\sqrt{6}}{2}\mathrm{i}\tilde{B}(\tilde{x}\mp\mathrm{i}\tilde{y})\tilde{\Psi}_{\pm1},\end{aligned}\tag{5}$$

where $\tilde{F}_z=2(|\tilde{\Psi}_2|^2-|\tilde{\Psi}_{-2}|^2)+|\tilde{\Psi}_1|^2-|\tilde{\Psi}_{-1}|^2$, $\tilde{F}_+=\tilde{F}_-^{\dagger}=2(\tilde{\Psi}_2^{\dagger}\tilde{\Psi}_1+\tilde{\Psi}_{-1}^{\dagger}\tilde{\Psi}_{-2})+\sqrt{6}(\tilde{\Psi}_1^{\dagger}\tilde{\Psi}_0+\tilde{\Psi}_0^{\dagger}\tilde{\Psi}_{-1})$, and $\tilde{V}_{\mathrm{ext}}=\frac{1}{2}(\tilde{x}^2+\tilde{y}^2)$. For simplicity, it will be convenient to drop off the tilde in the following calculation.

In order to quantitatively discuss the vortex solution, the coupled GP Eqs. (3)–(5) are solved by Crank–Nicolson method.[48] We have verified the stationary state solutions by starting the calculation from a variety of initial conditions, such as the Gaussian-like functions ($\Psi_l\sim\exp[-(x^2+y^2)/\alpha_l]$ with $l=\pm2,\pm1,0$ and α_l representing the width).

3. Results and discussion

3.1. Formation of the vortex chain

We firstly investigate the ground state in the ferromagnetic phase of spin-2 BECs with anisotropic SOC $\kappa_x = 1$ and $\kappa_y = 0$. Anisotropic SOC strength is fixed and IP magnetic field is not considered ($B = 0$). As shown in the 2D density distribution of Fig. 1(a), the rotation symmetry of the condensates is maintained and no density hole emerges because of the SOC effect. As depicted in the phase field of Fig. 1(b), the phases of different components change from $-\pi \to +\pi \to -\pi \cdots$ periodically. Obviously, anisotropic SOC could generate the plane wave ground state, which is similar to the Rashba-type SOC case.[49] No topological nontrivial excitations are generated with pure 1D SOC, while one kind of topological nontrivial excitation is triggered with the combined effect of 1D SOC and magnetic field. As shown in the 2D density distribution of Fig. 1(c), we can observe several density holes along the x-axis that are separated by density domains. The vortices can be identified in the phase image of every component of the BECs. From the phase field of Fig. 1(d), there are some phase singularities distributing along the x-axis and completely across the whole BECs. This new interesting configuration is referred to as the vortex chain, which essentially differs from the symmetric and equal distribution of vortices in the rotating BECs.[50] In the $y > 0$ region, there is a plane wave propagated toward the $-x$ direction. However, in the $y < 0$ region, there is a plane wave propagated toward the $+x$ direction. Apparently, the x-axis distributed phase singularities are attributed to the two contrary-propagated plane waves. The 1D vortex chain has been generated by SOC and rotation in the spin-1 BECs,[46] in which rotation could introduce canonical angular momentum to the system. However, the magnetic field in this calculation can work as "rotation" to introduce angular momentum when anisotropic SOC is considered (the effective rotation in the system depends on the gauge potential induced effective magnetic flux).[28]

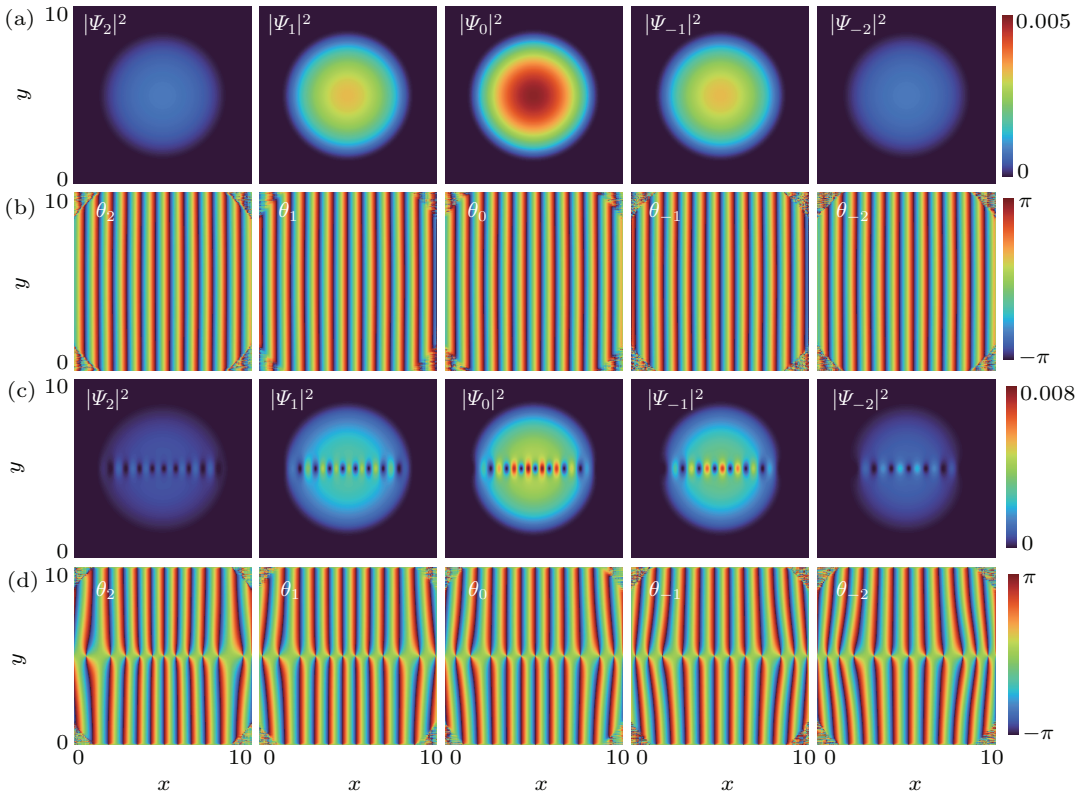


Fig. 1. The vortex chain is generated by anisotropic SOC and magnetic field. (a) The 2D density profiles of different components $|\Psi_l|^2$ ($l = \pm 2, \pm 1, 0$) when anisotropic SOC strength $\kappa_x = 1$, $\kappa_y = 0$ and magnetic field $B = 0$. (b) The corresponding phase fields θ_l are exhibited, which indicate the plane-wave ground state. (c) The 2D density profiles of different components $|\Psi_l|^2$ when anisotropic SOC strength $\kappa_x = 1$, $\kappa_y = 0$ and magnetic field $B = 0.25$. (d) The corresponding phase fields θ_l are exhibited, which indicate the vortex chain is distributed along the x-axis. In the GP simulation, the dimensionless density–density interaction $c_0 = 2500$, the spin-exchange interaction $c_1 = -50$, and the spin singlet-pairing $c_2 = 200$. Here, the length of the harmonic trap is $\xi_0 = \sqrt{\hbar/(m\omega_\perp)}$.

We can gain further insight into the discussed vortex chain solution by computing the canonical particle current density of the condensate[28]

$$J_l^c = -\frac{i\hbar}{2m}(\Psi_l^* \nabla \Psi_l - \Psi_l \nabla \Psi_l^*), \tag{6}$$

where $l = \pm 2, \pm 1, 0$ and m represents the atom mass. For the anisotropic SOC coupled BECs ($\kappa_x = 1$ and $\kappa_y = 0$) without magnetic field ($B = 0$), we display the canonical particle current of Ψ_{-2} component in Fig. 2(a) (the canonical particle currents of $\Psi_{2,1,0,-1}$ components share the similar configuration). Coincide with the phase field of different components in Fig. 1(b), the canonical particle current J_{-2}^c propagates to-

ward the $+x$ direction, indicating the plane wave ground state. Additionally, when magnetic field is considered ($B = 0.25$), anisotropic SOC could generate the vortex chain structure ($\kappa_x = 1$ and $\kappa_y = 0$), and the corresponding canonical particle current of Ψ_{-2} component is exhibited in Fig. 2(b). Along with the phase field in Fig. 1(d), the condensates are rotated by magnetic field, which results in the anticlockwise circulation of canonical particle current along the x-axis.

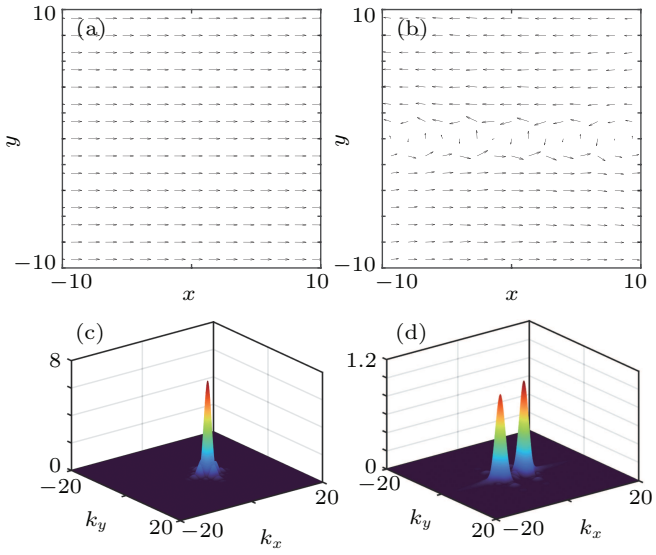


Fig. 2. The particle current and atomic momentum distribution of $|\Psi_{-2}|^2$ component. (a) The particle current of the plane wave phase ground state with magnetic field strength $B = 0$, anisotropic SOC strength $\kappa_x = 1$ and $\kappa_y = 0$. (b) The particle current of the vortex chain with magnetic field strength $B = 0.25$, anisotropic SOC strength $\kappa_x = 1$ and $\kappa_y = 0$. (c) The atomic momentum distribution of $|\Psi_{-2}(\boldsymbol{k})|^2$ with $B = 0$, $\kappa_x = 1$ and $\kappa_y = 0$. (d) The atomic momentum distribution of $|\Psi_{-2}(\boldsymbol{k})|^2$ with $B = 0.25$, $\kappa_x = 1$ and $\kappa_y = 0$. In the GP simulation, the dimensionless density–density interaction $c_0 = 2500$, the spin-exchange interaction $c_1 = -50$, and the spin singlet-pairing $c_2 = 200$. Here, the length of the harmonic trap is $\xi_0 = \sqrt{\hbar/(m\omega_\perp)}$.

In another vein, to better understand the physical meaning of the vortex chain, we transform the density profile of $|\Psi_{-2}(\boldsymbol{r})|^2$ into the momentum space $|\Psi_{-2}(\boldsymbol{k})|^2$ through Fourier transformation, as shown in Figs. 2(c) and 2(d). When anisotropic SOC strength $\kappa_x = 1$, $\kappa_y = 0$ and magnetic field strength $B = 0$, there is one localized Gaussian-type wave package distributing at $x > 0$ region, indicating a plane wave propagating toward the $+x$ direction (Fig. 2(c)). On the other hand, when anisotropic SOC strength $\kappa_x = 1$, $\kappa_y = 0$ and magnetic field strength $B = 0.25$, there are two localized Gaussian-type wave packages symmetrically distributing at both sides of the y-axis, implying two plane waves propagating toward the $+x$ and $-x$ directions, respectively (see Fig. 2(d)).

3.2. The vortex chain influenced by magnetic field

We next investigate the influence of the magnetic field on the vortex chain when anisotropic SOC is fixed as $\kappa_x = 1$ and $\kappa_y = 0$. As shown in Fig. 3(a), when magnetic field strength $B = 0$, different components exhibits Gaussian-type distribution without any density minimum. Meanwhile, the different components with opposite magnetic number (Ψ_{+2} and Ψ_{-2}, Ψ_{+1} and Ψ_{-1}) are totally overlapped, indicating zero magnetization. When magnetic field strength $B = 0.25$, the x-axis distributed vortex chain is formed, as depicted in Fig. 3(b). Different components are divided into continuous wave packages, and the different components with opposite magnetic quantum number are separated along the x-axis, indicating nonzero magnetization. In the 1D density profile, the density minima correspond to the position of the phase singularities exhibited in Fig. 1(d). The vortices continuously and homogeneously distribute along the x-axis, so we are willing to treat them as a whole vortex chain. Furthermore, the number of vortices in the vortex chain decreases with the strengthen of magnetic field. As shown in Figs. 3(c) and 3(d), the numbers of density minima in different components are decreased when magnetic field strength $B = 0.5$ and 0.75, respectively. We should notice that the number of vortices in a vortex chain is finite and intrinsic at the ground state with SOC and magnetic field. We can artificially change the intrinsic number of vortices inside the chain with different magnetic field strengths.

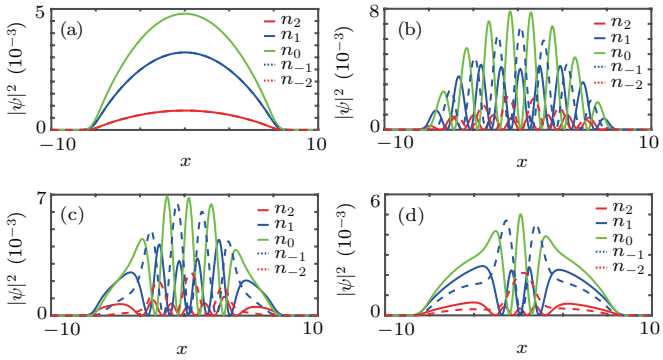


Fig. 3. Effect of magnetic field on the vortex chain in the anisotropic SO coupled BECs. (a) The 1D density profile of different components with magnetic field strength $B = 0$, anisotropic SOC strength $\kappa_x = 1$ and $\kappa_y = 0$. (b) The 1D density profile of different components with $B = 0.25$, $\kappa_x = 1$ and $\kappa_y = 0$. (c) The 1D density profile of different components with $B = 0.5$, $\kappa_x = 1$ and $\kappa_y = 0$. (d) The 1D density profile of different components with $B = 0.75$, $\kappa_x = 1$ and $\kappa_y = 0$. In the GP simulation, the dimensionless density–density interaction $c_0 = 2500$, the spin-exchange interaction $c_1 = -50$, and the spin singlet-pairing $c_2 = 200$. Here, the length of the harmonic trap is $\xi_0 = \sqrt{\hbar/(m\omega_\perp)}$.

3.3. The vortex chain influenced by anisotropic SOC

Furthermore, evolution of the vortex chain with anisotropic SOC is studied when magnetic field strength is fixed. We investigate the influence of 1D SOC on the vortex chain, which means $\kappa_y = 0$. For the reason that the different components share the similar density, phase field and momentum distribution, we only exhibit the distribution of Ψ_{-2} component for convenience. The momentum distribution of Ψ_{-2} component varies with the x-direction SOC strength, as depicted in Figs. 4(a)–4(d). When SOC strength $\kappa_x = 0.25$, as shown in Fig. 4(a), there are two localized wave packages localizing symmetrically on the both sides of the $k_x = 0$ line.

The overlap between the two momentum wave packages is obvious, and one vortex can be identified from the corresponding density contour (the vortex core is circled by the blue circular, and the red circular indicates the density domain). When SOC strength κ_x varies from $0.5 \to 1 \to 2$ in Figs. 4(b)–4(d), the distance between the two momentum wave packages becomes larger. The two localized momentum wave packages with no overlap corresponds to two plane waves propagated in the $+x$ and the $-x$ directions. From the corresponding density contours, we can identify an x-axis distributed vortex chain, in which the vortex number increases with SOC strength.

We next investigate the anisotropy of 2D SOC on the vortex chain, with x-direction SOC strength being fixed as $\kappa_x = 1$. When y-direction SOC strength is changed from 0 to 0.5 in Figs. 4(e) and 4(f), there is a small difference in the momentum distribution of Ψ_{-2} component. However, the corresponding density contours indicate the vortex number in the vortex chain decreases with the strengthen of κ_y. When the SOC strength is isotropy in Fig. 4(g), we can observe four momentum wave packages coupled together, and four vortices arranged in coaxial annular arrays. When $\kappa_y = 2$ in Fig. 4(h), two localized momentum wave packages are separated on both sides of the $k_y = 0$ line, corresponding to two plane waves propagating in the $+y$ and the $-y$ directions. Consequently, the vortex chain distributes along the y-axis.

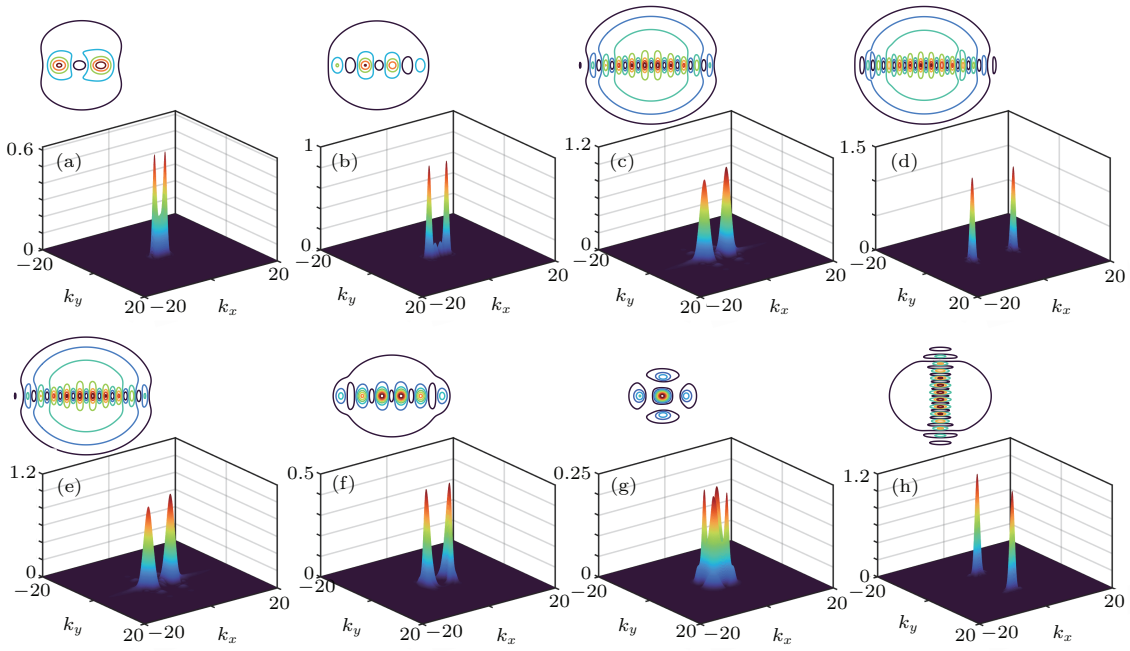


Fig. 4. Effect of anisotropic SOC on the vortex chain in the BECs system with a fixed magnetic field $B = 0.25$. The atomic momentum distribution of Ψ_{-2} component varies with 1D SOC $\kappa_x = 0.25$, $\kappa_y = 0$ in (a), $\kappa_x = 0.5$, $\kappa_y = 0$ in (b), $\kappa_x = 1$, $\kappa_y = 0$ in (c) and $\kappa_x = 2$, $\kappa_y = 0$ in (d). The atomic momentum distribution of Ψ_{-2} component varies with 2D SOC $\kappa_x = 1$, $\kappa_y = 0.25$ in (e), $\kappa_x = 1$, $\kappa_y = 0.5$ in (f), $\kappa_x = 1$, $\kappa_y = 1$ in (g) and $\kappa_x = 1$, $\kappa_y = 2$ in (h). The contour images correspond to the density distribution of Ψ_{-2} component. In the GP simulation, the dimensionless density–density interaction $c_0 = 2500$, the spin-exchange interaction $c_1 = -50$, and the spin singlet-pairing $c_2 = 200$. Here, the length of the harmonic trap is $\xi_0 = \sqrt{\hbar/(m\omega_\perp)}$.

3.4. Effect of atomic interactions

To connect with experiments, atomic interactions concerning magnetic orders should also be considered to influence the vortex chain. In spin-2 BECs, with the internal degree of freedom, atom collision interactions are generally spin dependent, i.e., the spin-dependent interactions (the spin-exchange interaction c_1 and the spin singlet-pairing interaction c_2) determine the phases of the ground states: ferromagnetic ($c_1 < 0$ and $c_2 > 0$), anti-ferromagnetic ($c_1 > 0$ and $c_2 < 0$) or the cyclic phase ($c_1 > 0$ and $c_2 > 0$).[51] When considering anisotropic SOC $\kappa_x = 1$ and $\kappa_y = 0$ in Figs. 5(a)–5(c), the momentum distribution of Ψ_{-2} components share the similar configuration for different phases. However, the density domains are elongated along the y-direction in the anti-ferromagnetic phase or cyclic phase comparing to the density domain in the ferromagnetic phase. When considering SOC $\kappa_x = 1$ and $\kappa_y = 1$ in Figs. 5(d)–5(f), the symmetry of the momentum distribution of Ψ_{-2} components are different for different phases: $SO(4)$ rotational symmetry in the ferromagnetic phase, $U(1)$ global gauge symmetry in the anti-ferromagnetic phase and $SO(3)$ rotational symmetry in the cyclic phase. Consequently, the density contour indicates that the density distribution is influenced by the atomic interaction. When considering anisotropic SOC $\kappa_x = 1$ and $\kappa_y = 2$ in Figs. 5(g)–5(i), the momentum distribution of Ψ_{-2} components share the similar configuration for different phases. However, the density domains are elongated along the x-direction in the anti-ferromagnetic phase and the cyclic phase comparing to the density domain in the ferromagnetic phase.

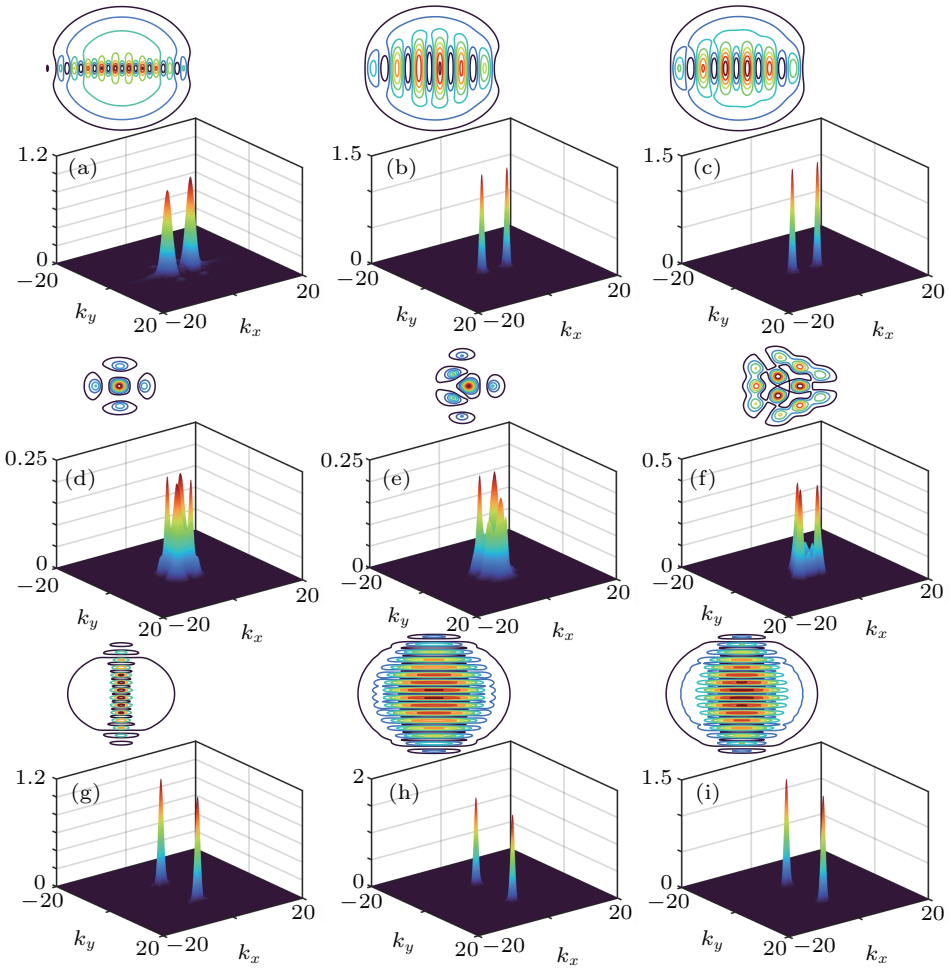


Fig. 5. The effect of atomic interaction effects on the vortex chain in the anisotropic SO coupled BECs system with magnetic field. When $\kappa_x = 1$, $\kappa_y = 0$ and $B = 0.25$, the atomic momentum distribution of Ψ_{-2} component varies with the spin-exchange interaction and the spin singlet-pairing interaction $c_1 = -50$, $c_2 = 200$ in (a), $c_1 = 50$, $c_2 = -200$ in (b), $c_1 = 50$, $c_2 = 50$ in (c). When $\kappa_x = 1$, $\kappa_y = 1$ and $B = 0.25$, the atomic momentum distribution of Ψ_{-2} component varies with $c_1 = -50$, $c_2 = 200$ in (d), $c_1 = 50$, $c_2 = -200$ in (e), $c_1 = 50$, $c_2 = 50$ in (f). When $\kappa_x = 1$, $\kappa_y = 2$ and $B = 0.25$, the atomic momentum distribution of Ψ_{-2} component varies with $c_1 = -50$, $c_2 = 200$ in (g), $c_1 = 50$, $c_2 = -200$ in (h), $c_1 = 50$, $c_2 = 50$ in (i). Here, the length of the harmonic trap is $\xi_0 = \sqrt{\hbar/(m\omega_\perp)}$.

4. Conclusion

We have investigated the anisotropic SO coupled spin-2 BECs with magnetic field by solving the coupled GP equations. The 1D vortex chain is generated by the combined effect of 1D SOC and magnetic field. The vortex chain is found to be the consequences of the domain wall of two opposite plane-wave phases. The magnetic effect mainly affects the number of vortices in the vortex chain. The anisotropy of SOC changes the vortex chain and causes the vortex lattice. Through varying the spin-exchange interaction and the spin singlet-pairing interaction, we find the different density profiles and momentum distributions of the vortex chain or the vortex lattice. This study provides exciting perspectives for nonlinear physics of condensates in artificially induced non-Abelian gauge fields.

Acknowledgments

Project supported by the National Key R&D Program of China (Grant No. 2016YFA0301500), the National Natural Science Foundation of China (Grant Nos. 61835013 and 11971067), Strategic Priority Research Program of the Chinese Academy of Sciences (Grant Nos. XDB01020300 and XDB21030300), Beijing Natural Science Foundation (Grant No. 1182009), and Beijing Great Wall Talents Cultivation Program (Grant No. CIT&TCD20180325).

References

[1] Durkin D and Fajans J 2000 *Phys. Rev. Lett.* **85** 4052
[2] Koshelev A E 2005 *Phys. Rev. B* **71** 174507
[3] Campbell L J 1989 *Phys. Rev. A* **39** 5436
[4] Eto M, Konishi K, Marmorini G, Nitta M, Ohashi K, Vinci K and Yokoi N 2006 *Phys. Rev. D* **74** 065021
[5] Hamner C, Zhang Y P, Chang J J, Zhang C W and Engels P 2013 *Phys. Rev. Lett.* **111** 264101
[6] Wen L H, Qiao Y J, Xu Y and Mao L 2013 *Phys. Rev. A* **87** 033604
[7] Churilov S and Stepanyants Y 2019 *Phys. Rev. Fluids* **4** 034704
[8] Ferreira C N, Helayël-Neto J A and Ney W G 2008 *Phys. Rev. D* **77** 105028
[9] Sadd M, Chester G V and Reatto L 1997 *Phys. Rev. Lett.* **79** 2490
[10] Lim L K, Smith C M and Hemmerich A 2008 *Phys. Rev. Lett.* **100** 130402
[11] Inui S, Nakagawa T and Tsubota M 2020 *Phys. Rev. B* **102** 224511
[12] Koshelev A E, Willa K, Willa R, Smylie M P, Bao J K, Chung D Y, Kanatzidis M G, Kwok W K and Welp U 2019 *Phys. Rev. B* **100** 094518

[13] Liarte D B, Hall D, Koufalis P N, Miyazaki A, Senanian A, Liepe L and Sethna J P 2018 *Phys. Rev. Appl.* **10** 054057
[14] Cooper N R 1999 *Phys. Rev. Lett.* **82** 1554
[15] Chanchal, Teja G P, Simon C and Goyal S K 2021 *Phys. Rev. A* **104** 043713
[16] Kapale K T and Dowling J P 2005 *Phys. Rev. Lett.* **95** 173601
[17] Yamaguchi T, Akashi N, Tsunegi S, Kubota H, Nakajima K and Taniguchi T 2020 *Phys. Rev. Research* **2** 023389
[18] Deng D, Lin M, Li Y and Zhao H 2019 *Phys. Rev. Applied* **12** 014048
[19] Ivanov I P 2012 *Phys. Rev. A* **85** 033813
[20] Simula T P, Petersen T C and Paganin D M 2013 *Phys. Rev. A* **88** 043626
[21] Sasaki K, Suzuki N, Akamatsu D and Saito H 2009 *Phys. Rev. A* **80** 063611
[22] Wright K C, Leslie L S, Hansen A and Bigelow N P 2009 *Phys. Rev. Lett.* **102** 030405
[23] McEndoo S and Busch T 2010 *Phys. Rev. A* **82** 013628
[24] Saarikoski H, Reimann S M, Räsänen E, Harju A and Puska M J 2005 *Phys. Rev. B* **71** 035421
[25] Cipriani M and Nitta M 2013 *Phys. Rev. A* **88** 013634
[26] Stringari S 2017 *Phys. Rev. Lett.* **118** 145302
[27] Qu C L and Stringari S 2018 *Phys. Rev. Lett.* **120** 183202
[28] Jin J J, Han W and Zhang S Y 2018 *Phys. Rev. A* **98** 063607
[29] Zhou X F, Zhou J and Wu C J 2011 *Phys. Rev. A* **84** 063624
[30] Madison K W, Chevy F, Wohlleben W and Dalibard J 2000 *Phys. Rev. Lett.* **84** 806
[31] Radić J, Sedrakyan T A, Spielman I B and Galitski V 2011 *Phys. Rev. A* **84** 063604
[32] Sinha S, Nath R and Santos L 2011 *Phys. Rev. Lett.* **107** 270401
[33] Zhou K Z and Zhang Z D 2012 *Phys. Rev. Lett.* **108** 025301
[34] Zhang Y P, Mao L and Zhang C W 2012 *Phys. Rev. Lett.* **108** 035302
[35] Xu X Q and Han J H 2011 *Phys. Rev. Lett.* **101** 200401
[36] Stanescu T D, Anderson B and Galitski V 2008 *Phys. Rev. A* **78** 023616
[37] Ozawa T and Baym G 2012 *Phys. Rev. A* **85** 013612
[38] Xu Z F, Lü R and You L 2011 *Phys. Rev. A* **83** 053602
[39] Liu C F, Fan H, Zhang Y C, Wang D S and Liu W M 2012 *Phys. Rev. A* **86** 053616
[40] Wang J G and Yang S J 2018 *J. Phys.: Condens. Matter* **30** 295404
[41] Wang J G and Li Y Q 2020 *Commun. Theor. Phys.* **72** 095701
[42] Xu Z F, Kawaguchi Y, You L and Ueda M 2012 *Phys. Rev. A* **86** 033628
[43] Saito H and Ueda M 2005 *Phys. Rev. A* **72** 053628
[44] Ueda M and Koashi M 2002 *Phys. Rev. A* **65** 063602
[45] Widera A, Gerbier F, Fölling S, Gericke T, Mandel O and Bloch I 2006 *New J. Phys.* **8** 152
[46] Liu C F, Yu Y M, Gou S C and Liu W M 2013 *Phys. Rev. A* **87** 063630
[47] Leanhardt A E, Görlitz A, Chikkatur A P, Kielpinski D, Shin Y, Pritchard D E and Ketterle W 2002 *Phys. Rev. Lett.* **89** 190403
[48] Leiler G and Rezzolla L 2006 *Phys. Rev. D* **73** 044001
[49] Wang C J, Gao G, Jian C M and Hui Zhai 2010 *Phys. Rev. Lett.* **105** 160403
[50] Mizushima T, Kobayashi N and Machida K 2004 *Phys. Rev. A* **70** 043613
[51] Kawaguchi Y and Ueda M 2012 *Phys. Rep.* **520** 253